Fighting SARS-CoV-2 with green seaweed *Ulva* sp. extract: extraction protocol predetermines crude ulvan extract anti-SARS-CoV-2 inhibition properties in *in vitro* Vero-E6 cells assay

Shai Shefer [Equal first author, 1], **Arthur Robin** [Equal first author, 1], **Alexander Chemodanov** [1], **Mario Lebendiker** [2], **Robert Bostwick** [3], **Lynn Rasmussen** [3], **Michael Lishner** [4], **Michael Gozin** [Corresp., 5], **Alexander Golberg** [Corresp. 1]

[1] Port School of Environment and Earth Sciences, Tel Aviv University, Tel Aviv, Israel

[2] Silberman Institute of Life Science, Hebrew University of Jerusalem, Jeruslem, Israel

[3] Sothern Research, Birmingham, Alabama, United States

[4] Meir Medical Center, Kvar Sava, Israel

[5] School of Chemisty, Tel Aviv University, Tel Aviv, Israel

Corresponding Authors: Michael Gozin, Alexander Golberg
Email address: cogozin@gmail.com, agolberg@tauex.tau.ac.il

Due to the global COVID19 pandemic, there is a need to screen for novel compounds with antiviral activity against SARS-COV-2. Here we compared chemical composition and the *in vitro* anti- SARS-COV-2 activity of two different *Ulva* sp. crude ulvan extracts: one obtained by an HCl-based and another one by ammonium oxalate-based (AOx) extraction protocols. The composition of the crude extracts was analyzed and their antiviral activity was assessed in a cytopathic effect reduction assay using Vero E6 cells. We show that the extraction protocols have a significant impact on the chemical composition, anti- SARS-COV-2 activity, and cytotoxicity of these ulvan extracts. The ulvan extract based on the AOx protocol had a higher average molecular weight, higher charge, and 11.3-fold higher antiviral activity than HCl-based extract. Our results strongly suggest that further bioassay-guided investigation into bioactivity of compounds found in*Ulva*sp. ulvan extracts could lead to the discovery of novel anti-SARS-CoV-2 antivirals.

Fighting SARS-CoV-2 with green seaweed *Ulva* sp. extract: extraction protocol predetermines crude ulvan extract anti-SARS-CoV-2 inhibition properties in *in vitro* Vero-E6 cells assay.

Shai Shefer,[1§] Arthur Robin,[1§] Alexander Chemodanov,[1] Mario Lebendiker,[2] Robert Bostwick[3], Lynn Rasmussen[3], Michael Lishner[4], Michael Gozin,[5]* Alexander Golberg[1]*

[1] Porter School of Environment and Earth Sciences, Faculty of Exact Sciences, Tel Aviv University, Tel Aviv

[2] Silberman Institute of Life Science. The Hebrew University of Jerusalem. Jerusalem. Israel.

[3] Sothern Research, Birmingham, Alabama, United States.

[4] Meir Medical Center, Kefar Sava, Israel.

[5] School of Chemistry, Faculty of Exact Sciences, Center for Nanoscience and Nanotechnology; Center for Advanced Combustion Science, Tel Aviv University, Tel Aviv, Israel.

[§] Equal first authors

* Correspondence should be addressed to Alexander Golberg, Email: agolberg@gmail.com and to Michael Gozin, Email: cogozin@gmail.com

Abstract

Due to the global COVID19 pandemic, there is a need to screen for novel compounds with antiviral activity against SARS-COV-2. Here we compared chemical composition and the *in vitro* anti- SARS-COV-2 activity of two different *Ulva* sp. crude ulvan extracts: one obtained by an HCl-based and another one by ammonium oxalate-based (AOx) extraction protocols. The composition of the crude extracts was analyzed and their antiviral activity was assessed in a cytopathic effect reduction assay using Vero E6 cells. We show that the extraction protocols have a significant impact on the chemical composition, anti- SARS-COV-2 activity, and cytotoxicity of these ulvan extracts. The ulvan extract based on the AOx protocol had a higher average molecular weight, higher charge, and 11.3-fold higher antiviral activity than HCl-based extract. Our results strongly suggest that further bioassay-guided investigation into bioactivity of compounds found in *Ulva* sp. ulvan extracts could lead to the discovery of novel anti-SARS-CoV-2 antivirals.

Keywords: SARS-CoV-2/covid19, antiviral, seaweed/macroalgae, sulfated polysaccharides, *Ulva* sp., extraction, ulvan

Introduction

The COVID-19 global pandemic is caused by SARS-COV-2 and its mutations, which infected more than 100 million and caused the death of more than 2 million people (World Health Organization, 21st January 2021). In addition to its fast propagation and lethality, COVID19 is causing a profound worldwide disruption of social and economic activities [1]. Moreover, serious post-illness long-term health damages were reported in many COVID-19 recovered patients [2,3]. Whereas the administration of new vaccines was initiated at the end of 2020 as a preventive measure against the spreading of the infection, alarming reports are being released regarding the potential of mutant strains to jeopardize both vaccine-based immunity and immunity developed from previous infections with the initial strains [4–7]. Presently, no broadly accepted and efficient anti-viral drug treatment for the COVID-19 has been implemented. . Thus, the need of finding new antiviral candidates is crucial for the treatment of SARS-COV-2[8].

A rich variety of synthetic compounds and biomolecules exhibit antiviral properties. Notably, a considerable amount of knowledge has been accumulated regarding antivirals that originated from terrestrial plants and organisms [9,10]. In contrast, the number of published articles that focused on antiviral biomolecules that originated from the marine environment is at least two orders of magnitude smaller than from terrestrial ones [9,11,12]. Out of the rich marine fauna and flora, macroalgae (or seaweed) are a large group of multicellular organisms encompassing several thousands of species, ranging from microscopic to large specimens of up to 30 m in length. Despite their diversity, macroalgae are much less explored than terrestrial organisms, while potentially containing numerous novel antivirals [13–15].

One of the significant differences between macroalgae and terrestrial and freshwater plants is the composition of their cell wall. More specifically, macroalgae differ from terrestrial plants in the chemical composition of their structural polysaccharides, many of which are sulfated [16]. Although the exact role of these seaweed sulfated polysaccharides (SSPS) is not determined, it was suggested that they can play a role in ion-exchange, nutrient binding, and concentration processes in the marine environment, as well as defense against pathogens and opportunistic organisms [17–19].

The inhibitory effects of SSPS on viral replication *in vitro* have been known for more than 60 years with activities against several enveloped RNA viruses, the family of the current source of pandemic SARS-CoV-2, such as HIV (various strains), Sindbis, Semliki forest, Junin, Tacaribe,

VSV, Influenza A, and RSV viruses[13–15,20–25]. As an example, SSPS was found to block HIV replication in cell cultures, at concentrations as low as 10 $\mu g \cdot ml^{-1}$ and without showing any toxicity to the host cells at concentrations of up to 2.5 $mg \cdot ml^{-1}$ [13,15]. The antiviral activities of such SSPS partially correlate with the presence of charged groups, mainly the sulfonate groups, which are present to a high degree in certain SSPS. However, the sulfonate group presence alone was not sufficient for explaining the antiviral activities of these compounds [14,22,23,26].

The interactions between virus envelope proteins and sulfated polymers are keys to the antiviral activity of the latter [13,15,26–29]. Besides a high charge density on the sulfated polymer, a high level of structural flexibility seems to be required for efficient binding of the polysaccharides to the protein located on the surface of viruses such as the dengue and SARS-COV2 viruses [26,27,29–31]. Thus, the inhibitory activity of the polysaccharides against SARS-CoV-2 may be also influenced by their structure[26,30–32]. The diversity of SSPS structures and sulfonate group content could be the main attributes behind those biopolymers' broad antiviral activity, which inspired several investigators to call for additional testing of SSPS against SARS-CoV2 [28,33,34]. Subsequently, iota-carrageenan and fucoidan SSPS, extracted from red and brown seaweeds, were found to have antiviral activity against SARS-CoV2, among other investigated sulfated polymers[29,32]. Although sulfated rhamans, part of ulvan polymers, found in green seaweed, were shown to have antiviral effects against a previous strain of human viruses such as corona and influenza viruses [23,25,35,36], there is no report regarding ulvan activity against SARS-CoV2.

Here we report on the anti-SARS-CoV-2 activity of two crude ulvans, extracted from a cultivated green seaweed *Ulva* sp., in an *in vitro* cytopathic effect (CPE) reduction assay using Vero E6 cells that are expressing angiotensin-converting enzyme 2 (ACE2) receptor to which SARS-CoV-2 virus typically binds [37,38]. These two extracts of ulvan, a known SSPS of *Ulva* sp. green seaweed, were obtained by two different extraction protocols, namely an HCl- and an ammonium oxalate. Extraction protocols greatly affect the quantity and quality of the ulvan extracts, notably their purity, molecular weight distribution, sulfate content, and bioactivity [39] The advantage of using *Ulva* sp. is in the possibility of controlling SSPS content and composition under-regulated growth conditions [40,41]. As presently, there is no accepted and efficient treatment for the SARS-COV-2, and there is still a need for new antiviral therapeutics, we believe this work provides essential information for further development of natural product-based therapeutic agents against SARS-CoV-2 and its mutants' pandemics [42].

Materials and Methods

Ulva sp. biomass cultivation

Green macroalgae *Ulva sp*. was grown under controlled media from April to May 2020 and illumination conditions, using macroalgae photobioreactors (MPBR) [41]. In terms of the taxonomic status, the used macroalgae contained a mixture of *Ulva rigida* and *Ulva fasciata* [43]. The growth media was based on Mediterranean seawater, to which ammonium nitrate (NH_4NO_3) and phosphoric acid (H_3PO_4) (Haifa Chemicals Ltd., Israel) were added, to adjust total nitrogen and phosphorous contents to 6.4 and 0.97 $g \cdot m^{-3}$, respectively, and pH to 8.2. Throughout the biomass cultivation, agitation and CO_2 were provided by air bubbling at a flow rate of 2-4 $L \cdot min^{-1}$. Before further use, fresh *Ulva sp*. biomass was harvested, washed from minerals and epiphytes with deionized water, and centrifuged at 2,800 rpm to remove the excess of water.

Ulvan extraction

Extraction with Ammonium Oxalate (AOx Protocol). A crude extraction of the ulvan from tap water washed *Ulva sp*. biomass was carried out according to a modified Robic's protocol [44]. First, the biomass was ground with an addition of deionized water to form a wet homogeneous paste, from which surplus water was removed by squeezing it out in a filter bag. Then, from the resulted wet material, pigments were extracted with ethanol at room temperature. Following ethanol treatment, filtering, and air drying, ulvan was extracted for 2 hrs with a vigorously stirred hot solution (75 ± 5 °C) of aqueous ammonium oxalate ($[NH_4]_2[C_2O_4]$, 20 mM, pH 7) [19]. After that time, the supernatant was collected by centrifugation and its volume was reduced by 90 % on a rotary evaporator at 60 ± 5 °C / 60 mmHg. To obtain a dry extract, the concentrated supernatant solution was dialyzed against deionized water, using 3.5 kDa dialysis membranes for 24 hrs, and was subsequently lyophilized. The resulting dry ulvan powder was further sterilized with a low-intensity γ-irradiation treatment (25 kGy [45], Soreq Nuclear Research Center, Israel) and kept at -20°C before further use.

Extraction with Aqueous Hydrochloric Acid (HCl Protocol). The solid material resulting from ethanol treatment, filtering, and air drying was suspended in deionized water (1:30 w/v) and the pH of this suspension was adjusted to 2.0-2.5 (at room temperature) by dropwise addition of aqueous HCl (5 %). As in the previous protocol, hot extraction (75 ± 5 °C) of ulvan was conducted

for 2 hrs with vigorous stirring (inspired by Kidgell, 2019[39]). After that time, the resulted mixture was cooled down to room temperature, and solid residues were removed first by filtration through a "parachute silk" (woven nylon) filter and then by subsequent centrifugation at 4,000 rpm (15 min, 4 °C). Subsequently, the supernatant was adjusted to a neutral pH by dropwise addition of aqueous NaOH (2.0 M), and the volume of the supernatant was reduced by 90 % on a rotary evaporator at 60 ± 5 °C/ 60 mmHg. As previously mentioned, the dry extract was obtained by dialysis of the concentrated supernatant against deionized water, followed by lyophilization. The resulting dry ulvan powder was sterilized by γ-irradiation and kept at -20°C before further use.

Elemental and FTIR Analyses

Elemental analyses of solid freeze-dried ulvan extract samples were performed on a CHNS elemental analyzer (Flash2000, Thermo Scientific) at the Schulich Faculty of Chemistry of the Technion (Haifa, Israel). FT-IR spectroscopy analyses of the solid freeze-dried ulvan extract samples were performed on a spectrometer (Tensor 27, Bruker) equipped with a standard attenuated total reflection attachment (ATR, Pike). FT-IR spectra of the extracts were measured in the spectral range of 4000-400 cm^{-1} (4 cm^{-1} resolution). Samples we analyzed at least in a duplicate.

Size Exclusion and Anion Exchange Chromatography

Sample Preparation for Chromatography. A sample of solid ulvan extract (20 mg) was suspended in HPLC-grade water (20 mL) and kept for 10 min at RT. Then, the undissolved solids were removed by centrifugation (13,000 rpm) and the resulted supernatant was further filtered through a 0.22 μm filter (PVDF, Merck).

Size Exclusion Chromatography (SEC) Analysis. SEC analyses were performed at room temperature on a system (AKTA Pure, Cytiva), equipped with Superose 6 Increase 10/300 GL column (23 ml, Cytiva) and with an array of detectors, comprised of UV-vis detector (UV-900, Cytiva), a multi-angle light scattering (MALS; miniDAWN TREOS, Wyatt Technology) detector, a dynamic light scattering module (WyattQELS) and with a refractive index detector (Optilab T-rEX, Wyatt Technology). The elution was monitored at 280, 260, and 220 nm (UV-vis detector) and three angles (43.6°, 90°, and 136.4°) with a 658.9 nm laser beam (MALS detector) [46]. The refractive index of the eluting solvent was determined to be 1.331, the viscosity was 0.8945 cP

(typical for the PBS buffer) and the refractive index increment value (d_n/d_c) for ulvan was defined to be 0.127 $mL \cdot g^{-1}$ [47]. The data collection and analyses were performed with ASTRA 6.1 software (Wyatt Technology). A sample (with a typical volume of 0.5 mL) was injected into the column equilibrated with an eluent comprised of MES buffer (10 mM, pH 6.0) and NaCl (50 mM). A typical flow rate was 0.8 $mL \cdot min^{-1}$ and for molecular weight (MW) calibration of this column see Table S1 (Supporting Information).

Anion Exclusion Chromatography (AEX) Analysis. AEX analyses were performed at room temperature on aforementioned system (AKTA Pure, Cytiva) equipped with a high resolution, anion exchange Mono-Q HR 5/5 column (1 mL, Cytiva) and with the same array of detectors [46,48]. For AEX analysis, a sample of PVDF filtered extract (0.5 mL) was diluted ten-fold with eluent A (sodium acetate buffer, 20 mM, pH 5.0) and injected (5 mL) into the Mono-Q HR 5/5 column equilibrated with the eluent A. Typical separation conditions included a gradient elution (with a flow rate of 1.5 $mL \cdot min^{-1}$) starting with an eluent A and gradual increase in sodium chloride concentration to an eluent B (sodium chloride, 2.0 M; sodium acetate buffer, 20 mM, pH 5.0). The elution was conducted at room temperature in the following sequence: (i) an initial isocratic elution with 15 column volumes (cv) of the eluent A (100 %), (ii) followed by a gradient elution with 25 cv of eluent A/eluent B mixture (from 100%/0% to 75%/25%), (iii) followed by an isocratic elution with 15 cv of eluent A/eluent B mixture (75%/25%), (iv) followed by a gradient elution with 10 cv of eluent A/eluent B mixture (from 75%/25% to 0%/100%) and (v) completed by an isocratic elution with 7 cv of eluent B (100 %). It should be mentioned that significant changes in sodium chloride concentration, during the gradient elution can affect the baseline calibration of certain MALS detectors, introducing errors to the calculations of the radius of gyration (R_g). This issue could be alleviated with the use of multiple angles MALS detectors. Optilab T-rEX detector allows effective RI detection up to a sodium chloride concentration of 0.5 M, above which (at higher conductivity), RI signal could not be properly detected in our system.

Cytopathic Effects of the Ulvan Extracts in Vero E6 Cell Assay for SARS-CoV-2

Cytopathic Effect (CPE) Assay with Vero E6 Cells: The assay was performed by the Southern Research (Birmingham, AL) High-Throughput Screening Center. Mammalian Vero E6 cells selected for this CPE assay were capable of expression of the angiotensin-converting enzyme 2 (ACE2) receptor to which SARS-CoV-2 typically binds [37]. The Vero E6 cells were obtained from

Dr. Ralph Baric at the University of North Carolina. Vero E6 cells were grown in Minimum Essential Media (MEM) supplemented with 10% of Heat-Inactivated Fetal Bovine Serum (HI FBS). On the day of assay, the cells were harvested with MEM supplemented with 1% Pen/Strep and 2% HI FBS. Subsequently, the harvested cells were batch inoculated with SARS-CoV-2 virus (strain USA-WA12020) having a Multiplicity of Infection (MOI) ratio of 0.002. This inoculation resulted in 5% of cells' post-infection viability after 72 hrs. Assay Ready Plates (ARPs, 384-well plate, Corning 3712BC) were prepared in a BioSafety Laboratory level 2 (BSL-2) facility, by adding 5 µL of analyzed samples to the ARPs. In control wells, only MEM supplemented with HI FBS (5 µL) was added. Then, these ARPs were transferred to a BioSafety Laboratory level 3 (BSL-3) facility, where 25 µL aliquots of SARS-CoV-2 virus inoculated cells were added to each well (4,000 Vero E6 cells per well), bringing the total volume per well of 30 µL. After incubating ARPs at 37 °C/5% CO_2 and 90 % humidity for 72 hrs, 30 µL of Cell Titer-Glo (Promega) was added to each well. To measure cells' viability, following incubation at room temperature for 10 min., the luminescence was measured by using a plate reader (Perkin Elmer Envision). Positive control compounds, with known *in vitro* anti-viral effects against SARS-CoV-2, were also tested in this assay. These reference compounds included Calpain Inhibitor IV, chloroquine, Remdesivir, hydroxychloroquine, and Aloxistatin (E64d).

Sample Preparation for the CPE Assay: A solid sample of ulvan extract was resuspended in MEM supplemented with 2% HI FBS solution to a concentration of 30 $mg \cdot mL^{-1}$. It was then kept for 10 min at RT, centrifuged (13,000 rpm), and filtered through a 0.22 µm filter. The resulted stock solution was used for the preparation of the diluted samples. Subsequently, a series of dilutions was performed in which the stock solution was diluted 3-fold (per dilution) 9 times, providing 10 different concentrations of an extract in a range between 30 $mg \cdot mL^{-1}$ and 1.52 $\mu g \cdot mL^{-1}$. In the ARPs, after the addition of the cells' solutions in media (25 µL), these 10 different concentrations were further diluted 6-fold, making the final concentration range of the assayed ulvan extract between 5 $mg \cdot ml^{-1}$ to 0.25 $\mu g \cdot mL^{-1}$. This specific concentration range was chosen to encompass both the cytotoxicity level (in a range of $mg \cdot mL^{-1}$) and potential acute anti-viral activity (in a range of $\mu g \cdot mL^{-1}$), as was reported for assays of other viruses [15,30].

Measurement of Cytotoxicity Effect of Ulvan Extracts: For measurement of the cytotoxicity effect of various ulvan extracts, the method for sample preparation and assay included all the above-described steps, except for the step in which the virus was inoculated. The cytotoxicity of

different ulvan extracts was evaluated by adding 25 µl aliquot of cells, without viruses, to 5 µl of ulvan extracts and to control wells containing only cell media. After incubating these ARPs at 37 °C/5% CO_2 under 90 % humidity for 72 hrs, 30 µL of Cell Titer-Glo (Promega) was added to each well. To measure cells' viability, following incubation at room temperature for 10 min., the luminescence was measured by using a plate reader (BMG CLARIOstar). For each plate, positive control with known *in vitro* cytotoxic effect against Vero E6 cells (*N*-benzyl-*N, N*-dimethyl-2-{2-[4-(2,4,4-trimethyl-pentan-2-yl)phenoxy]-ethoxy}ethanaminium chloride; hyaline, 100 µM) was added. Each analysis was performed in two duplicate wells.

Assays' Output Processing: Data from the plate reader were normalized to the average signal obtained from wells containing uninfected cells (*Avg Cells*, **Equation 1**), corresponding to 100 % virus inhibition result. The average signal obtained from wells containing virus-infected cells (*Avg Virus*, **Equation 1**) is corresponding to a 0 % virus inhibition result (wells to which no ulvan extracts or any other reference antiviral compounds were added). The tested compound (*Test Cmpd*, **Equation 1**) parameter is defined as the average signal obtained from the wells containing a sample of analyzed ulvan extract. To calculate [*% Inhibition*] values in the CPE assay, we used, **Equation 1**:

$$\% \, Inhibition = 100 \times \frac{(Test \; Cmpd \; - \; Avg \; Virus)}{(Avg \; Cells \; - \; Avg \; Virus)} \qquad (1)$$

The output signal which is coming from the wells containing only the Vero E6 cells is defined as the highest output signal (*Control*; **Equation 2**), corresponding to the 100% cell viability. The output signal coming from the wells containing the hyamine-treated cells is defined as the lowest output signal (*Avg Hyamine*; **Equation 2**), corresponding to the 0% cell viability and the highest cytotoxic effect in this assay. To calculate [*% Cell Viability*] values in the cytotoxicity assay, we used **Equation 2**:

$$\% \, Cell \, Viability \; = 100 \times \frac{(Test \; Cmpd - Avg \; Hyamine)}{(Control - Avg \; Hyamine)} \qquad (2)$$

The values of the half-maximum viral inhibitory concentration (IC_{50}) and the half-maximum cytotoxicity concentration (CC_{50}) were obtained by using non-linear regression, fitting the

concentration-response titration data into 4-parameters Hill equation, allowing us to determine the IC_{50}, CC_{50}, and the Selectivity Index ($SI = CC_{50}/IC_{50}$) values for AOx and HCl ulvan extracts.

Results and Discussion

Our project focused on the cultivation, extraction, bioassay, and chemical analysis of green seaweed *Ulva sp*. ulvan extracts. The lab cultivation was preferred to reduce to the minimum various contaminations in the *Ulva sp*. biomass, which may come from its native marine habitat. By controlling the light exposure, nutrients composition, aeration, and temperature, the lab cultivation of the *Ulva* sp. could allow for better control over variability in the resulted biomass composition in future commercial production.

Bioassay of Extracts.

In this study, we used a Cytopathic Effect (CPE) reduction assay, performed with mammalian Vero E6 cells that were infected with the SARS-CoV-2 virus. This type of essay is popular and widely used for screening agents for their antiviral activity [49]. CPE assay allows to correctly evaluate the broad antiviral activity potential of tested material, regardless of the inhibited infection stage, such as virus binding to host cell receptor, entering the host cells, replication, assembly, budding, and reinfection of neighboring cells. In our CPE assay, the mammalian Vero E6 host cells, capable of expressing the angiotensin-converting enzyme 2 (ACE2) receptor, to which SARS-CoV-2 typically bind, were inoculated with this virus. The virus utilizes the host cell machinery for its replication and spreading, ultimately leading to the death of the infected cell. Efficient antivirals are not cytotoxic and are capable of maintaining the viability of the SARS-CoV-2 inoculated cells from the cytopathic effect of the virus. For the CPE assay, Vero E6 cells inoculated with SARS-CoV-2 virus were grown in media containing various concentrations of the tested compounds. The cell viability was assessed after 72 hrs of incubation. The assay boundaries were the viability of the uninoculated Vero E6 cells, which represent 100% inhibition of the virus activity, and untreated cells inoculated with the SARS-CoV-2 virus, which represent 0% inhibition (virus-induced cell's death). To test the cytotoxicity of our ulvan extracts against Vero E6 cells, we compared them, in the absence of SARS-CoV-2 virus, to a known cytotoxic reference compound – *N*-benzyl-*N, N*-dimethyl-2-{2-[4-(2,4,4-trimethyl-pentan-2-yl)phenoxy]-ethoxy}ethanaminium chloride (hyamine). The activity of *Ulva* sp. crude ulvan extracts was compared to a series of reference synthetic antivirals, which were shown to be active against

SARS-CoV-2 virus *in vitro*, including Calpain Inhibitor IV, chloroquine, Remdesivir, hydroxychloroquine, and Aloxistatin (E64d) (**Table 1**) [50].

We found that AOx ulvan extract showed anti-SARS-CoV-2 positive activity (**IC_{50}** 4.14 mg·mL^{-1}) with some cytotoxic effects (CC_{50} 3.58 mg·mL^{-1}) (**Table 1, Figure 1**). The Vero E6 cells viability in the AOx ulvan extract experiment was about 70 %, which is 14 times higher than the same cell viability observed in the negative control experiment, which included inoculation with the virus. In contrast, even at its maximum tested concentration (5.00 mg·mL), the HCl-based extract did not show any inhibition of the SARS-CoV-2 virus in the CPE assay, while having the same cytotoxic activity (3.58 mg·mL^{-1}) as the AOx-based extract.

Table 1

Figure 1

These data show that the AOx-based extract exhibited apparent anti-viral activity against SARS CoV-2, albeit only at the highest permissible concentration (5 mg/ml) tested in the assay, achieving a 75% reduction of the virus-induced cytopathic effect. At this same concentration, the AOx-extract reduced the viability of uninfected host cells to 50% of that measured in untreated control wells. Thus, the reduction in virus-induced CPE may be a consequence of the effect of the extract on the health of host cells, compromising their ability to support viral replication. However, the observation that the HCl extract exhibited a similar cytotoxic effect on the host cell could not yet reduce CPE suggests that the cytotoxic effect *per se* is not the reason for CPE reduction.

We suggest that the inhibition of SARS-CoV-2 induced CPE in Vero E6 cells is due to an antiviral activity of the AOx-based extract. Whether this effect results from direct action on the virus or is mediated through a host cell target needs to be elucidated in follow up studies. Regarding a host target, it will be necessary to evaluate antiviral activity in assays using cells from the human lung which is a major site of virus infection. In addition, assay with TMPRSS2 should be used for further screening. To the best of our knowledge, this is the first report of *Ulva* sp.-derived crude extract bioactivity against the SARS-CoV-2. Although the *in vitro* potency of the AOx-based extract in this assay is much lower (IC50 = 4.14 mg·mL^{-1}) compared to the small organic antiviral molecules tested in parallel (IC50 = 4.00 to 18.08 µg·mL^{-1}; **Table 1**), the active component(s) of

the AOx-extract needs to be purified and might be more potent in assays that directly measure virus load and replication [50,51].

Chemical Characterization of Extracts.

In an attempt to find differences in the chemical composition of HCl- and AOx-based ulvan extracts, we analyzed these materials by combustion elemental analysis of carbon, hydrogen, nitrogen, and sulfur elements (CHNS analysis, **Figure 2**). The results of the CHNS analysis of materials obtained by both extraction protocols showed a close content similarity for carbon, hydrogen, and sulfur elements. The main difference between the two types of extracts was observed in the nitrogen content of the resulted materials, which was 88 % higher in the case of AOx-based protocol. This result suggests a higher protein content in the AOx protocol-derived material, indicating that under neutral pH conditions of the AOx extraction more proteins underwent co-extraction with sulfated polysaccharides [39,52,53]. In the case of the HCl-based protocol, at acid pH conditions most of the proteins are found to be poorly soluble and thus remain in the solid residues [39]. Besides, it is plausible that a higher degree of protein hydrolysis to amino acids and peptides also took place at pH 2 and 75°C. These low MW compounds were subsequently removed by dialysis during the purification of the extracts.

The sulfur content in both types of extracts is important, as most of the previous literature regarding the antiviral activity of seaweed sulfated polysaccharides showed a good correlation between the higher sulfur content of the evaluated material and its higher bioactivity [15,26,28,30]. Since in our case, the sulfur content in both types of extracts was practically identical (**Figure 2**), a possible antiviral activity of the AOx extract may come from differences in the polysaccharides' structures and/or due to the formation of protein- polysaccharides complexes and aggregates.

Figure 2

In addition to the elemental analysis, both extracts (in their lyophilized form) were analyzed by the attenuated total reflection Fourier transform infrared spectroscopy (ATR-FTIR; **Figure 3**). The FTIR spectra of materials obtained from HCl- and AOx-based extraction were quite typical to the spectra of ulvans extracted from different species of Ulva *sp*. and by different extraction protocols [53].

Both measured FTIR spectra for the HCl- and AOx-protocols exhibited a high degree of similarity, especially for the following peaks: 848 cm^{-1} (corresponding to the stretching of C-O-S bonds, usually found in ulvan, due to the presence of the sulfate groups), 983 cm^{-1} (corresponding to the stretching of C-O bonds in sugars), 1,215 cm^{-1} (corresponding to the stretching of S=O bond of the sulfate groups) and 1,600 cm^{-1} (corresponding to the carboxylic groups of the uronic acid moieties). Major differences between our FTIR spectra were found in the intensities of the peaks, which were stronger for the material produced by the HCl-protocol. These include peaks at 573 cm^{-1}, 1,032 cm^{-1} (corresponding to the symmetric stretching of C-O-C bonds of carboxylic groups), 1,425 cm^{-1} (corresponding to the asymmetric stretching of O-C-O bonds of carboxylic groups), 2,940 cm^{-1} (corresponding to the stretching of C-H bond) and around 3,375 cm^{-1} (corresponding to the O-H stretching of the hydroxyl groups). Only small differences were present between the FTIR spectra of the HCl and AOx extracts, and it was found to be closely similar to the FTIR spectra of a reference commercial "winter-heavy" ulvan (by CarboSynth, UK) extracted from *Ulva* armoricana collected in Bretagne, France [53]. Overall, all our extracted ulvans showed similar absorbance profiles to previously published FTIR spectra of ulvan [54].

Figure 3.

Fraction analysis of the extracts

Generally, ulvan extracts contain branched polysaccharides with a broad distribution in terms of their charge density and MW [39,53–55]. Also, ulvan extracts can contain minor quantities of proteins, nucleic acids, phenolic compounds, and metal salts. For a better characterization of our extracts, we performed chromatographic separation by mass / hydrodynamic radius using Size Exclusion Chromatography (SEC), or by charge using Anion Exchange Chromatography (AEIX). The elution was monitored by Diode-Array UV detector, coupled with multi-angle light scattering (MALS) and Refraction Index (RI) detectors.

SEC Analysis

SEC-analysis of the two crude ulvan extracts showed significant differences in composition (**Figure 4**). Absorbance at 280 nm in both samples of AOx (**Figure 4A**) and HCl extracts (**Figure 4B**), indicated the presence of proteins in the analyzed samples. This absorbance was detected

throughout the entire sample elution, starting from the void volume (minor quantities) and gradually increasing until the end of the elution (larger quantities). However, the absorbance at 280 nm in the chromatogram of the AOx extract exhibited two unseparated peaks eluting between 7 to 11 mL, which were practically not present in the chromatogram of the HCl extract.

The chromatogram of the AOx extract monitored by the RI detector exhibited a profile with two unseparated peaks, where the higher peak eluted between 7 to 11 mL elution volumes, and the smaller one eluted between 11 to 18 mL elution volumes. The chromatogram of the HCl extract monitored by the RI detector showed a different profile, with a unique broad peak eluting between 12 to 18 mL elution volumes. These two chromatogram profiles indicated the presence of a wide distribution of MW and/or chemical compositions in the polysaccharide extracts. They also revealed a profound difference in the composition of the two extracts. Each of the chromatograms of the two extracts, monitored by the LS detector, showed a strong peak eluting between 7 to 11 mL elution volumes. It could be attributed to the higher sensitivity of such detector to high MW polysaccharides in comparison to low MW polysaccharides, even if the latter is in higher concentration.

Overall, higher signals as monitored by the LS detector was observed in the chromatogram of the AOx extract than in the chromatogram of the HCl extract. The LS/RI profile indicated the presence of branched polysaccharides with a broad distribution of MW in the fractionation range of the SEC analytical column (Superose 6 Increase), i.e. from 5 to 5,000 kDa. Three populations of average MWs could be distinguished in each SEC chromatogram (black curves in **Figures 4A** and **4B**). More specifically, we are referring to the fractions with an average molecular weight of 9.48×10^7 and 1.62×10^7 g·mol^{-1} for the first eluting fraction (between 7 to 9 mL elution volumes), 3.45×10^6 and 1.16×10^6 g·mol^{-1} for the second eluting fraction (between 9 to 11 mL elution volumes), and 4.21×10^5 and 4.20×10^4 g·mol^{-1} for the third eluting fraction (between 11 to 17 mL elution volumes), for the AOx and HCl extracts, respectively. For all three populations, the average MWs were significantly higher in the AOx extract (**Figure 4A**) than in the HCl extract (**Figure 4B**). Extraction at acidic conditions at a temperature above 70°C seemed to induce minor hydrolysis of the extracted SSPS leading to a corresponding minor reduction in the obtained average MWs by SEC compared to the extraction at neutral pH (AOx protocol). Those results are consistent with previous reports that acid extraction protocols yield lower MW polysaccharides than with other ammonium oxalate-based protocols [39,54,55]. Calculations of the average MWs by

the software (ASTRA) should be analyzed with the recognition of the limitations of the light-scattering detector utilized in the present work. The latter is a tri-angle light scattering detector, which is not as accurate as a multi-angle detector for measuring the MW of mixtures with a complex chemical composition including branched polymers. It is noteworthy to mention that the void volume of the used SEC column is around 7 mL, its total volume is 23 mL, and what is eluting after 18 mL are very low MW molecules that are below the fractionation range of the column. Thus, the peaks monitored by the RI and UV detectors after the elution of 18 mL are referring to materials with an average MW below 5 kDa and therefore not relevant for the SEC analysis of our polysaccharides of interest. The analysis by SEC revealed differences in the MW distribution in the two extracts. The difference in chemical composition between the two extracts was then investigated using AEX, which is a more suitable tool for the fractionation of mixtures of charged polymers.

Figure 4

AEX Analysis

Ulvan contains two types of negatively charged groups: sulfate esters (on rhamnose and xylose moieties) and carboxylate groups (glucuronic or iduronic acids moieties) that are distributed in repeating disaccharides structures, as described in **Figure 5** [39,53]. The presence of these charged groups allows the fractionation of the two SPSS extracts by the anion-exchange chromatography. For our extracts, a relatively low pH (5.0) was used to reduce the strong binding of the negatively charged polysaccharides to the used AEX column. Fractionation of Ulvan extracts was achieved by using a strong anion exchange Mono-Q column, utilizing eluent with gradually increased concentration of sodium chloride (from 0 mM to 2 M) in sodium acetate buffer (20 mM, pH 5.0).

Figure 5

AEX chromatograms of SSPS extract from Ulva *sp*., obtained from AOx (**Figure 6A**) and HCl protocols (**Figure 6B**), respectively, show substantial differences in the composition of the extracted materials. As monitored by the UV detector at 220 nm, the main eluted peaks which are corresponding to 5 different fractions of organic materials in these extracts, were identified according to their volume of elution and named in their order of elution: from **P1** to **P5** (**Figure 6**). The first peak (**P1**, **Figures 6A** and **6B**) was eluted at 16 mL (at the concentration of NaCl of 28 mM) and corresponded to the elution of the void volume.

Notably, the AEX chromatogram monitored by the UV detector at 260 and 280 nm of the AOx extract showed apparent nucleic acids/proteins peaks (with a prevalence of the former as suggested by the ratio of the absorbance at 260 and 280 nm) at around an elution volume of 20 mL, corresponding to the eluting peaks between **P1** and **P2** (**Figure 6A**) at the gradient condition of NaCl of about 110 mM, at 39 mL (**P3**, NaCl 480 mM), 55.5 mL (**P4**, NaCl 800 mM), and at 58.5 mL (**P5**, ~1 M NaCl). In comparison, the number of proteins and nucleic acids was much lower in the chromatogram of the HCl extract, with a small wide peak eluting from 19.6 mL (NaCl ~100 mM) to 39 mL (NaCl 480 mM) and a second narrower peak at 55.5 mL (**P5**, NaCl ~800 mM) (**Figure 6B**).

Analyzing signals from the UV detector at 220, 260, and 280 nm, we concluded that the peaks **P3** and **P4** could be attributed to proteins and nucleic acid contaminants. Those two peaks were absent in the chromatogram of the HCl extracts and we can conclude that the HCl protocol yielded an extract of SSPS with higher purity, in comparison to the AOx extraction protocol. These results were in line with the higher nitrogen content observed in the abovementioned results of CHNS analysis, and with previous reports comparing the extraction of SSPS from *Ulva* sp. biomass with similar protocols [39]. Thus, only the materials eluted at peaks **P1**, **P2,** and **P5** are of interest, as their UV signal corresponded to potential fractions of polysaccharides.

The monitoring of UV absorbance at 280 nm and LS and Dynamic Light Scattering (QELS) signals during the analysis are showed for the AOx (**Figure 6C**) and HCl (**Figure 6D**) extracts, respectively. Nevertheless, the peaks in the LS chromatogram showed the presence of high MW polysaccharides, eluting from 58 mL at NaCl concentration of 1 M, in both extracts; although the intensity of the signal was much higher in the chromatogram of the AOx extract in comparison to the HCl extract. Those MW polysaccharides that were tightly bonded to the AEX column seemed to refer to the targeted sulfated polysaccharides ulvan in the two extracts.

We hypothesize that **P1** and **P2** peaks correspond to low MW polysaccharides (eluting with other contaminants) that are not retained on the column, nor detected by the LS detector. Only **P5** peak was observed in the chromatogram of the AOx extract (**Figure 6C**), while in the chromatogram of the HCl extract a small additional peak shoulder P6 was visible (at a similar elution volume of **P4**), before the elution of the main **P5** peak (**Figure 6D**). The latter two peaks indicated the presence of two different populations of SSPS that could be separated by their different interactions with the AEX column, where the shoulder peak has fewer negatively charged

groups than in the main peak **P5**. In comparison, only **P5** could be observed in the chromatograms of the AOx extract as monitored by the LS and QELS detector (**Figure 6C**). The peak **P4** is present on the UV absorbance chromatograms but not on the LS and QELS chromatograms. This result suggests that the composition of the materials eluting at the volume corresponding to **P4** and **P6** is different. Overall, based on SEC and AEX analyses, the HCl extraction protocol produced more homogeneous material. However, the amount of the latter material was smaller than in the case of more heterogeneous mixture l obtained by the AOx extraction protocol.

Figure 6

Based on the CHNS, FTIR, SEC, and AEX analyses, we found that the AOx and HCl extraction protocols of *Ulva* sp. resulted in mixtures of compounds having a different distribution of molecular weights, overall molecular charges, and contaminations level with nitrogen-containing molecules. Remarkably, both these extracts had also somewhat different antiviral activity, confirming our initial hypothesis regarding the variability in the biological activity of SSPS compounds obtained by different extraction protocols. Our idea for testing the SSPS of the green seaweed *Ulva* sp. as a potential candidate against SARS-CoV-2 was based on previously reported antiviral activities of SSPS [27,29,32]. In this work, we show that the AOx extracts indeed showed a positive *in vitro* antiviral activity, protecting VERO E6 cells against the cytopathic effect of the SARS-CoV-2. Our observations are in line with existing hypotheses that the antiviral activity of SSPS against SARS-CoV-2 and other viruses could be attributed to the interaction of the negatively charged groups of SSPS polysaccharides with proteins located on the envelope of viruses [26,29,30]. These interactions could be also influenced by charge density on SSPS biopolymers, their MWs, and the flexibility of the polysaccharide backbone, as we found that AOx-based extract had a higher average MW (*versus* HCl-based extract), a higher overall charge, and a more potent antiviral activity. We should mention that the IC_{50} of the AOx-based extract was in the concentration range of a few $mg \cdot ml^{-1}$, while previously reported antiviral activity of ulvan was in the range of tens of $\mu g \cdot ml^{-1}$ [21,23,36].

Our results indicate that either the activity of the AOx-based extract against SARS-CoV-2 was not as potent as other SSPS against other viruses, or, most probably, only a specific fraction of this AOx-based extract is active against SARS-CoV-2. The latter possibility is strongly supported by

reports regarding various fractions isolated from SSPS extracts exhibiting significantly different antiviral activities [23,36]. Since the cytotoxicity of compounds obtained in the AOx- and HCl-based extraction protocols were closely comparable, yet, had an 11.3-fold difference in their maximum inhibition activity against SARS-CoV-2, it is reasonable to conclude that the antiviral activity of the AOx-based extracts may originate from a specific type of compounds found in sufficient quantity in the latter extract, but not present in the HCl-based extracts. In line with this conclusion, we found that the AOx-based extracts also exhibited a higher level of nitrogen-containing compounds, in comparison to the HCl-based extracts. Although the presence of nitrogen-containing molecules in our extraction protocols was minimized by dialysis and other purification steps, nitrogen-containing molecules could be still present in our extracts due to their strong affinity to the SSPS [39,44]. These nitrogen-containing molecules could be secondary metabolites, such as alkaloids, various peptides, proteins, and even fragments of nucleic acids, and they could be responsible for the difference of antiviral activity in the two extracts. For example, recently, an alkaloid caulerpin, isolated from a green seaweed Caulerpa *sp.*, was predicted *in silico* to have potent anti-SARS-CoV2 activity [56]. More interestingly, lectins, a group of carbohydrate-binding proteins with antiviral activities (including against SARS-CoV-2) are present in the *Ulva* sp. cell wall and could thus be co-extracted with the SSPS [57–60].

Conclusions

In this work, we provide experimental data regarding the inhibition of SARS-CoV-2 by ulvan crude extract. We compared chemical composition and bioactivity of crude extracts obtained from an HCl-based and an ammonium oxalate-based (AOx) extraction protocols, using green seaweed *Ulva sp*. as a source of the SSPS ulvan. The composition of materials obtained by both extraction protocols was analyzed by infrared spectroscopy, CHNS elemental analysis, size exclusion (SEC), and ion exchange (AEC) chromatography, while the antiviral activity evaluation of these compounds was performed in a cytopathic assay on VERO E6 cells. The main conclusions of our study were that the extraction protocol had a significant impact on the chemical composition of the extracted SSPS, which included variations in molecular weight distribution, charge, and the level of nitrogen-containing contaminations. Also, there was a significant difference in the antiviral activity of the two extracts which could be due to the difference in chemical composition. The AOx-based extract was found to have higher average molecular weight, stronger charges, and

higher antiviral activity *versus* HCl-based extract. Yet, the AOx-based extract had a more heterogeneous composition.

Although specific isolation and precise identification of the active components in the AOx-based extract is still required, we suggest that our present work will serve as a starting point for a thorough bioassay-guided fractionation approach. Despite worldwide vaccination campaigns, it is crucial to continue the efforts in the discovery of new antiviral therapeutic agents. One of the major reasons is the continuous appearance of new virus mutants some of which exhibiting resistance to both vaccine-based immunity and known antivirals. The second reason is related to the antiviral activity of certain SSPS, which are offering a vast chemical library and a platform for the development of broadly active antivirals, with potential high specific activity against certain viruses, including variants of known viruses.

References

(the mention: "**(**NOT PEER-REVIEWED**)**" is used to indicated non-peer-reviewed references).

1. Nicola M, Alsafi Z, Sohrabi C, et al. The socio-economic implications of the coronavirus pandemic (COVID-19): A review. *Int J Surg*. 2020;78:185.

2. Mitrani RD, Dabas N, Goldberger JJ. COVID-19 cardiac injury: implications for long-term surveillance and outcomes in survivors. *Hear Rhythm*. 2020.

3. Balachandar V, Mahalaxmi I, Devi SM, et al. Follow-up studies in COVID-19 recovered patients-is it mandatory? *Sci Total Environ*. 2020:139021.

4. Baum A, Fulton BO, Wloga E, et al. Antibody cocktail to SARS-CoV-2 spike protein prevents rapid mutational escape seen with individual antibodies. *Science (80-)*. 2020;369(6506):1014 LP - 1018. doi:10.1126/science.abd0831

5. **(**NOT PEER-REVIEWED**)** Nelson G, Buzko O, Spilman P, Niazi K, Rabizadeh S, Soon-Shiong P. Molecular dynamic simulation reveals E484K mutation enhances spike RBD-ACE2 affinity and the combination of E484K, K417N and N501Y mutations (501Y.V2 variant) induces conformational change greater than N501Y mutant alone, potentially resulting in an escap. *bioRxiv*. January 2021:2021.01.13.426558. doi:10.1101/2021.01.13.426558

6. Zhang J, Ding N, Ren L, et al. COVID-19 reinfection in the presence of neutralizing antibodies. *Natl Sci Rev*. January 2021. doi:10.1093/nsr/nwab006

7. Wibmer CK, Ayres F, Hermanus T, et al. SARS-CoV-2 501Y.V2 escapes neutralization by South African COVID-19 donor plasma. *Nature Medicine* 2021 (27): 622–625 doi:10.1101/2021.01.18.427166

8. Hilgenfeld R, Peiris M. From SARS to MERS: 10 years of research on highly pathogenic human coronaviruses. *Antiviral Res*. 2013;100(1):286-295. doi:10.1016/J.ANTIVIRAL.2013.08.015

9. Li S, Chen C, Zhang H, et al. Identification of natural compounds with antiviral activities against SARS-associated coronavirus. *Antiviral Res*. 2005;67(1):18-23.

10. Hudson JB. *Antiviral Compounds from Plants*. CRC Press; 2018.

11. Uzair B, Mahmood Z, Tabassum S. Antiviral activity of natural products extracted from marine organisms. *BioImpacts BI*. 2011;1(4):203.

12. Donia M, Hamann MT. Marine natural products and their potential applications as anti-infective agents. *Lancet Infect Dis*. 2003;3(6):338-348.

13. Luescher-Mattli M. Algae, A Possible Source for New Drugs in the Treatment of HIV and Other Viral Diseases. *Curr Med Chem - Anti-Infective Agents*. 2003;2(3):219-225. doi:http://dx.doi.org/10.2174/1568012033483051

14. Pujol CA, Carlucci MJ, Matulewicz MC, Damonte EB. Natural Sulfated Polysaccharides for the Prevention and Control of Viral Infections. In: Khan MTH, ed. Berlin, Heidelberg: Springer Berlin Heidelberg; 2007:259-281. doi:10.1007/7081_2007_080

15. Witvrouw M, De Clercq E. Sulfated Polysaccharides Extracted from Sea Algae as Potential Antiviral Drugs. *Gen Pharmacol Vasc Syst*. 1997;29(4):497-511. doi:10.1016/S0306-3623(96)00563-0

16. Jiao G, Yu G, Zhang J, Ewart HS. Chemical Structures and Bioactivities of Sulfated Polysaccharides from Marine Algae. *Mar Drugs*. 2011;9(2):196-223. doi:10.3390/md9020196

17. Kloareg B, Quatrano RS. Structure of the cell walls of marine algae and ecophysiological

functions of the matrix polysaccharides. *Oceanogr Mar Biol AN Annu Rev*. 1988;26:259-315.

18. Ingle KN, Polikovsky M, Chemodanov A, Golberg A. Marine integrated pest management (MIPM) approach for sustainable seagriculture. *Algal Res*. 2018;29:223-232. doi:10.1016/j.algal.2017.11.010

19. Alves A, Sousa RA, Reis RL. A practical perspective on ulvan extracted from green algae. *J Appl Phycol*. 2013;25(2):407-424. doi:10.1007/s10811-012-9875-4

20. Gerber P, Dutcher JD, Adams E V, Sherman JH. Protective effect of seaweed extracts for chicken embryos infected with influenza B or mumps virus. *Proc Soc Exp Biol Med*. 1958;99(3):590-593.

21. Chiu Y-H, Chan Y-L, Li T-L, Wu C-J. Inhibition of Japanese Encephalitis Virus Infection by the Sulfated Polysaccharide Extracts from Ulva lactuca. *Mar Biotechnol*. 2012;14(4):468-478. doi:10.1007/s10126-011-9428-x

22. Hayashi K, Hamada J, Hayashi T. A Screening Strategy for Selection of Anti-HSV-1 and Anti-HIV Extracts from Algae. *Phyther Res*. 1996;10(3):233-237.

23. Lee J-B, Hayashi K, Maeda M, Hayashi T. Antiherpetic activities of sulfated polysaccharides from green algae. *Planta Med*. 2004;70(09):813-817.

24. Besednova NN, Makarenkova ID, Zvyagintseva TN, Imbs TI, Somova LM, Zaporozhets TS. Antiviral activity and pathogenetic targets for seaweed sulfated polysaccharides in herpesvirus infections. *Biochem Suppl Ser B Biomed Chem*. 2016;10(1):31-42. doi:10.1134/S1990750816010029

25. Terasawa M, Hayashi K, Lee J-B, et al. Anti-Influenza A Virus Activity of Rhamnan Sulfate from Green Algae Monostroma nitidum in Mice with Normal and Compromised Immunity. *Mar Drugs* . 2020;18(5). doi:10.3390/md18050254

26. Ghosh T, Chattopadhyay K, Marschall M, Karmakar P, Mandal P, Ray B. Focus on antivirally active sulfated polysaccharides: From structure–activity analysis to clinical evaluation. *Glycobiology*. 2009;19(1):2-15. doi:10.1093/glycob/cwn092

628 27. Jin W, Zhang W, Mitra D, et al. The structure-activity relationship of the interactions of
629 SARS-CoV-2 spike glycoproteins with glucuronomannan and sulfated galactofucan from
630 Saccharina japonica. *Int J Biol Macromol*. 2020;163:1649-1658.
631 doi:https://doi.org/10.1016/j.ijbiomac.2020.09.184

632 28. Chen X, Han W, Wang G, Zhao X. Application prospect of polysaccharides in the
633 development of anti-novel coronavirus drugs and vaccines. *Int J Biol Macromol*.
634 2020;164:331-343. doi:https://doi.org/10.1016/j.ijbiomac.2020.07.106

635 29. Song S, Peng H, Wang Q, et al. Inhibitory activities of marine sulfated polysaccharides
636 against SARS-CoV-2. *Food Funct*. 2020;11(9):7415-7420.

637 30. Damonte EB, Matulewicz MC, Cerezo AS. Sulfated seaweed polysaccharides as antiviral
638 agents. *Curr Med Chem*. 2004;11(18):2399-2419.

639 31. Marks RM, Lu H, Sundaresan R, et al. Probing the Interaction of Dengue Virus Envelope
640 Protein with Heparin: Assessment of Glycosaminoglycan-Derived Inhibitors. *J Med*
641 *Chem*. 2001;44(13):2178-2187. doi:10.1021/jm000412i

642 32. Kwon PS, Oh H, Kwon S-J, et al. Sulfated polysaccharides effectively inhibit SARS-CoV-
643 2 in vitro. *Cell Discov*. 2020;6(1):50. doi:10.1038/s41421-020-00192-8

644 33. Pereira L, Critchley AT. The COVID 19 novel coronavirus pandemic 2020: seaweeds to
645 the rescue? Why does substantial, supporting research about the antiviral properties of
646 seaweed polysaccharides seem to go unrecognized by the pharmaceutical community in
647 these desperate times? *J Appl Phycol*. 2020:1.

648 34. Bhatt A, Arora P, Prajapati SK. Can Algal Derived Bioactive Metabolites Serve as
649 Potential Therapeutics for the Treatment of SARS-CoV-2 Like Viral Infection? *Front*
650 *Microbiol*. 2020;11:596374. doi:10.3389/fmicb.2020.596374

651 35. Kyoko H, Toshimitsu H, Jung-bum L. *Evaluation of Anti-Human Coronavirus Agents*
652 *(Funded Project Details and Report)*.; 2006. https://kaken.nii.ac.jp/en/grant/KAKENHI-
653 PROJECT-16590434/.

654 36. Lopes N, Ray S, Espada SF, et al. Green seaweed Enteromorpha compressa (Chlorophyta,
655 Ulvaceae) derived sulphated polysaccharides inhibit herpes simplex virus. *Int J Biol*

656 *Macromol*. 2017;102:605-612.

657 37. Lan J, Ge J, Yu J, et al. Structure of the SARS-CoV-2 spike receptor-binding domain
658 bound to the ACE2 receptor. *Nature*. 2020;581(7807):215-220.

659 38. Li W, Moore MJ, Vasilieva N, et al. Angiotensin-converting enzyme 2 is a functional
660 receptor for the SARS coronavirus. *Nature*. 2003;426(6965):450-454.

661 39. Kidgell JT, Magnusson M, de Nys R, Glasson CRK. Ulvan: A systematic review of
662 extraction, composition and function. *Algal Res*. 2019;39:101422.
663 doi:10.1016/J.ALGAL.2019.101422

664 40. Robin A, Chavel P, Chemodanov A, Israel A, Golberg A. Diversity of monosaccharides in
665 marine macroalgae from the Eastern Mediterranean Sea. *Algal Res*. 2017;28:118-127.
666 doi:10.1016/j.algal.2017.10.005

667 41. Chemodanov A, Robin A, Golberg A. Design of marine macroalgae photobioreactor
668 integrated into building to support seagriculture for biorefinery and bioeconomy.
669 *Bioresour Technol*. 2017;241:1084-1093.
670 http://www.sciencedirect.com/science/article/pii/S0960852417309628.

671 42. Lahlou M. The Success of Natural Products in Drug Discovery. *Pharmacol &*
672 *Pharm*. 2013. doi:10.4236/pp.2013.43a003

673 43. Nimrod Krupnik BR, Paz G, Douek J, et al. Native, invasive and cryptogenic Ulva species
674 from the Israeli Mediterranean Sea: risk and potential. *Mediterr Mar Sci*. 2018;19(1):132-
675 146. doi:http://dx.doi.org/10.12681/mms.2104

676 44. Robic A, Rondeau-Mouro C, Sassi JF, Lerat Y, Lahaye M. Structure and interactions of
677 ulvan in the cell wall of the marine green algae Ulva rotundata (Ulvales, Chlorophyceae).
678 *Carbohydr Polym*. 2009;77(2):206-216.
679 doi:http://dx.doi.org/10.1016/j.carbpol.2008.12.023

680 45. Munarin F, Bozzini S, Visai L, Tanzi MC, Petrini P. Food Hydrocolloids Sterilization
681 treatments on polysaccharides : Effects and side effects on pectin. *Food Hydrocoll*.
682 2013;31(1):74-84. doi:10.1016/j.foodhyd.2012.09.017

46. Amartely H, Some D, Tsadok A, Lebendiker M. Ion Exchange Chromatography (IEX) Coupled to Multi-angle Light Scattering (MALS) for Protein Separation and Characterization. *JoVE (Journal Vis Exp*. 2019;(146):e59408.

47. Paradossi G, Cavalieri F, Chiessi E. A conformational study on the algal polysaccharide ulvan. *Macromolecules*. 2002;35(16):6404-6411.

48. Amartely H, Avraham O, Friedler A, Livnah O, Lebendiker M. Coupling multi angle light scattering to ion exchange chromatography (IEX-MALS) for protein characterization. *Sci Rep*. 2018;8(1):1-9.

49. Heaton NS. Revisiting the concept of a cytopathic viral infection. *PLoS Pathog*. 2017;13(7):e1006409.

50. Chen CZ, Shinn P, Itkin Z, et al. Drug repurposing screen for compounds inhibiting the cytopathic effect of SARS-CoV-2. *Front Pharmacol. 2020; 11: 592737.*.

51. **(**NOT PEER-REVIEWED**)** Gorshkov K, Chen CZ, Bostwick R, et al. The SARS-CoV-2 cytopathic effect is blocked with autophagy modulators. *bioRxiv Prepr Serv Biol*. May 2020:2020.05.16.091520. doi:10.1101/2020.05.16.091520

52. Glasson CRK, Sims IM, Carnachan SM, de Nys R, Magnusson M. A cascading biorefinery process targeting sulfated polysaccharides (ulvan) from Ulva ohnoi. *Algal Res*. 2017;27(May):383-391. doi:10.1016/j.algal.2017.07.001

53. Wahlström N, Nylander F, Malmhäll-Bah E, et al. Composition and structure of cell wall ulvans recovered from Ulva spp. along the Swedish west coast. *Carbohydr Polym*. 2020;233:115852.

54. Robic A, Bertrand D, Sassi J-FF, Lerat Y, Lahaye M. Determination of the chemical composition of ulvan, a cell wall polysaccharide from Ulva spp. (Ulvales, Chlorophyta) by FT-IR and chemometrics. *J Appl Phycol*. 2009;21(4):451-456. doi:10.1007/s10811-008-9390-9

55. Robic A, Gaillard C, Sassi J, Lerat Y, Lahaye M. Ultrastructure of ulvan: a polysaccharide from green seaweeds. *Biopolym Orig Res Biomol*. 2009;91(8):652-664.

56. Ahmed SA, Abdelrheem DA, El-Mageed HRA, et al. Destabilizing the structural integrity

of COVID-19 by caulerpin and its derivatives along with some antiviral drugs: An in silico approaches for a combination therapy. *Struct Chem*. 2020;31(6):2391-2412. doi:10.1007/s11224-020-01586-w

57. Barre A, Damme EJM Van, Simplicien M, Benoist H, Rougé P. Man-Specific, GalNAc/T/Tn-Specific and Neu5Ac-Specific Seaweed Lectins as Glycan Probes for the SARS-CoV-2 (COVID-19) Coronavirus. *Mar Drugs* . 2020;18(11). doi:10.3390/md18110543

58. Wang S, Zhong F-D, Zhang Y-J, Wu Z-J, Lin Q-Y, Xie L-H. Molecular Characterization of a New Lectin from the Marine Alga Ulva pertusa. *Acta Biochim Biophys Sin (Shanghai)*. 2004;36(2):111-117. doi:10.1093/abbs/36.2.111

59. Liu Y-M, Shahed-Al-Mahmud M, Chen X, et al. A Carbohydrate-Binding Protein from the Edible Lablab Beans Effectively Blocks the Infections of Influenza Viruses and SARS-CoV-2. *Cell Rep*. 2020;32(6):108016. doi:https://doi.org/10.1016/j.celrep.2020.108016

60. Mitchell CA, Ramessar K, O'Keefe BR. Antiviral lectins: Selective inhibitors of viral entry. *Antiviral Res*. 2017;142:37-54.

Table 1(on next page)

Summary of CPE assay with Vero E6 host cells for anti-SARS-CoV-2 ulvans crude extract activity.

Table 1. Summary of CPE assay with Vero E6 host cells for anti-SARS-CoV-2 ulvans crude extract activity.

Compound	Activity Against SARS-CoV-2	Max% Inhibition	IC_{50}	CC_{50}	Cytotoxic Activity	Min % Viability
Ulvan (by HCl Protocol)	Inactive	6.65	> 5.00 mg·mL^{-1}	3.75 mg·mL^{-1}	Active	38.17
Ulvan (by AOx Protocol)	**Active**	75.28	4.14 mg·mL^{-1}	3.58 mg·mL^{-1}	**Active**	50.81
Calpain Inhibitor IV	Active	113.79	0.131 µg·mL^{-1}	> 4.00 µg·mL^{-1}	Inactive	95.21
Chloroquine	Active	103.85	1.184 µg·mL^{-1}	> 9.60 µg·mL^{-1}	Inactive	93.95
Remdesivir	Active	103.02	2.944 µg·mL^{-1}	> 18.08 µg·mL^{-1}	Inactive	92.7
Hydroxychloroquine	Active	101.33	1.865 µg·mL^{-1}	> 10.08 µg·mL^{-1}	Inactive	94.19
Aloxistatin (E64d)	Active	74.58	4.908 µg·mL^{-1}	> 10.27 µg·mL^{-1}	Inactive	92.78

Figure 1

SARS-CoV-2 infection inhibition in Vero E6 cells with ulvan

Percentage of inhibition of SARS-CoV-2 virus in Vero E6 cells in the CPE assay, *Ulva sp.* extracts: by AOx Protocol (dashed dark red curve, with ● dots); by HCl Protocol (solid red curve, with ▲ dots). Percentage of the viability of the Vero E6 cells in the cytotoxicity assay, of *Ulva sp.* extracts: by AOx Protocol (dashed black curve, with ● dots); by HCl Protocol (solid black curve, with ▲ dots). For each concentration, measured in duplicates, curves were drawn using Locally Estimated Scatterplot Smoothing methodology.

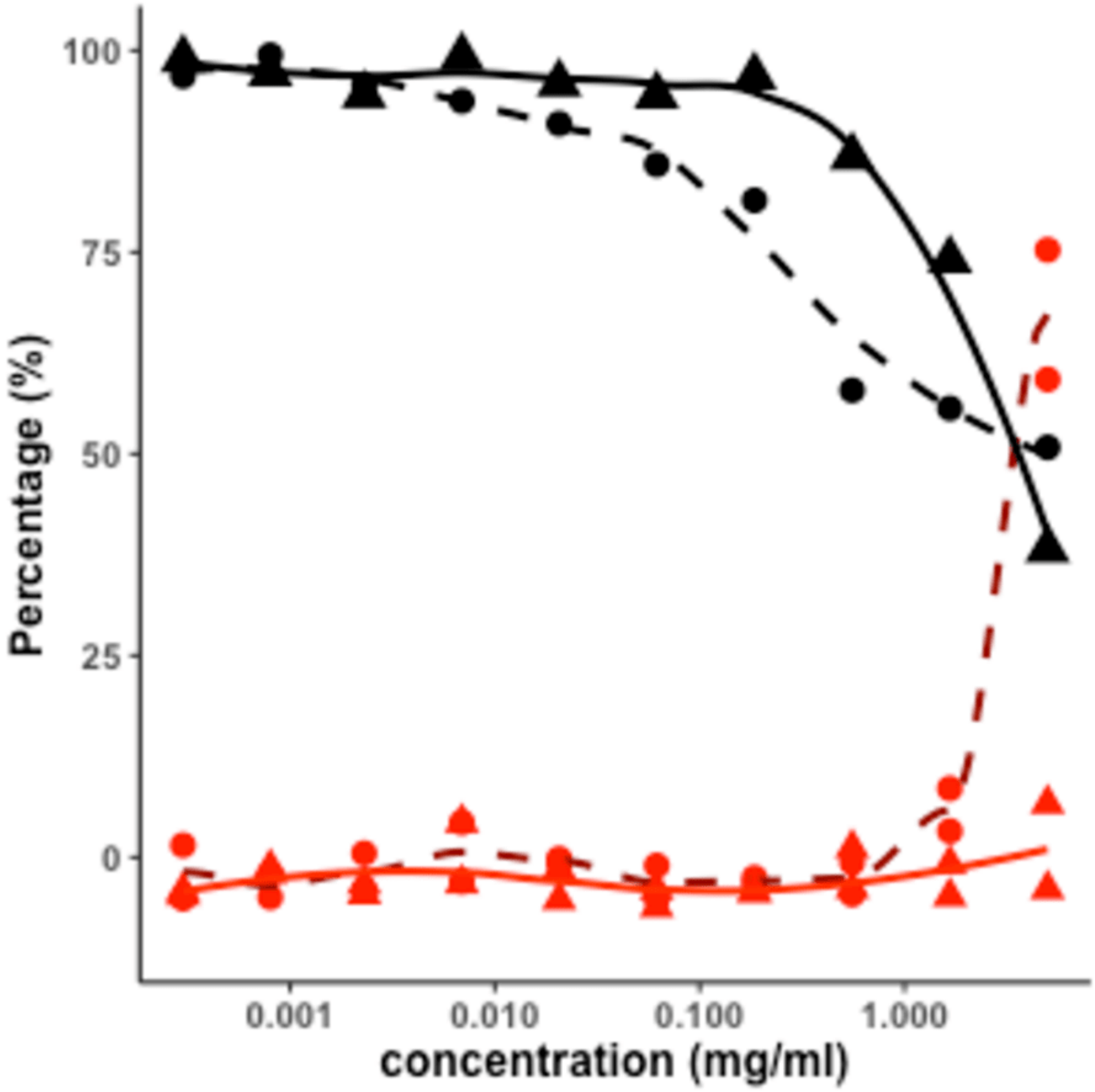
100
75
50
25
0
Percentage (%)
0.001
0.010
0.100
1.000
concentration (mg/ml)

Figure 2

Ulvan elemental analysis

CHNS elemental analysis of the two *Ulva* sp. ulvan extracts. (*red columns*): extraction by HCl protocol and (blue columns): extraction by AOx protocol.

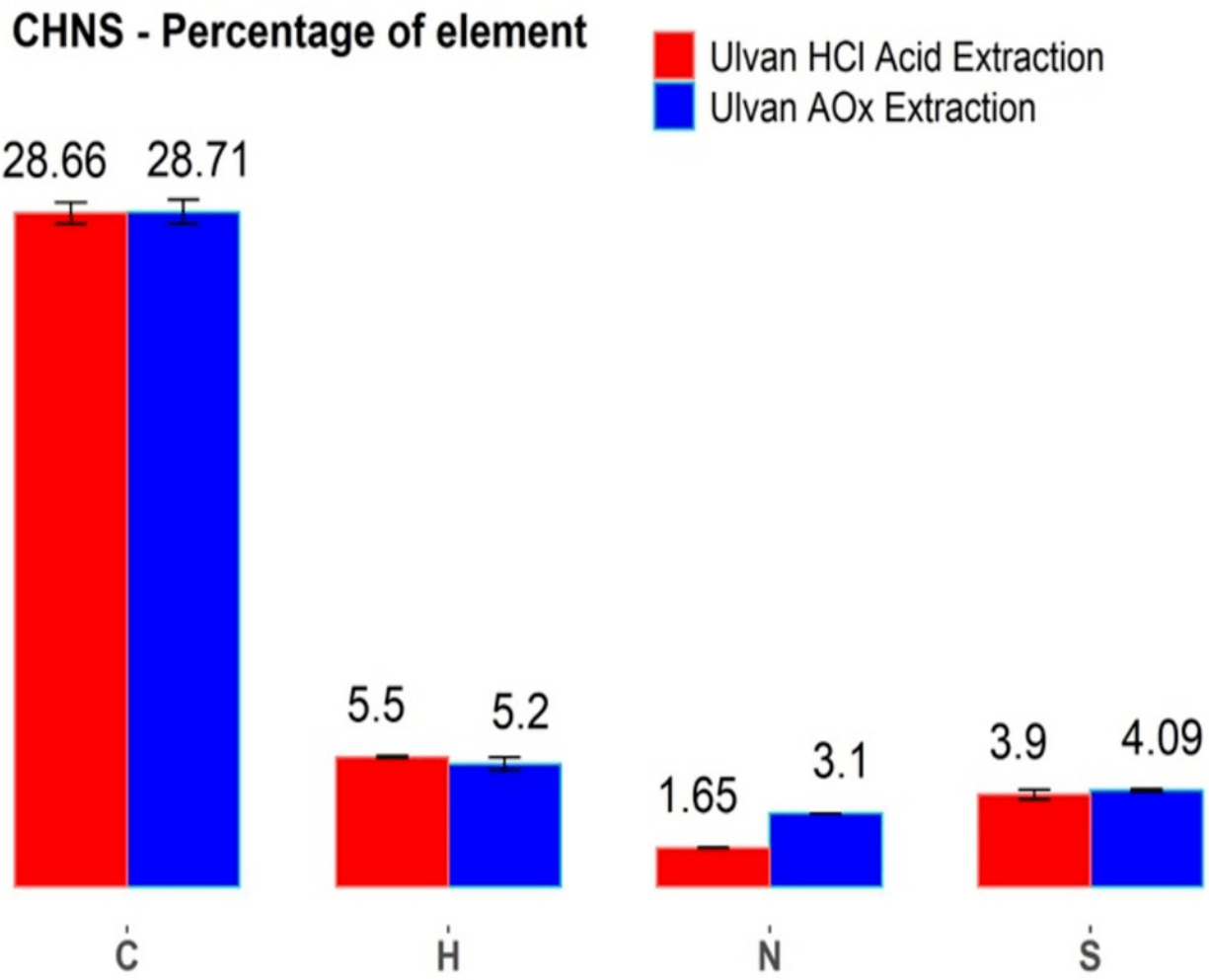

Figure 3

Fourier-transform infrared spectroscopy (FTIR) of ulvans

FTIR spectra of extracted ulvan from *Ulva* sp. Top spectra: (blue spectrum): material obtained in HCl-based extraction; (red spectrum): material obtained in ammonium oxalate-based extraction. Bottom spectra: reference spectra of ulvan from Ulva armoricana, adapted from Wahlström (2020) 53.

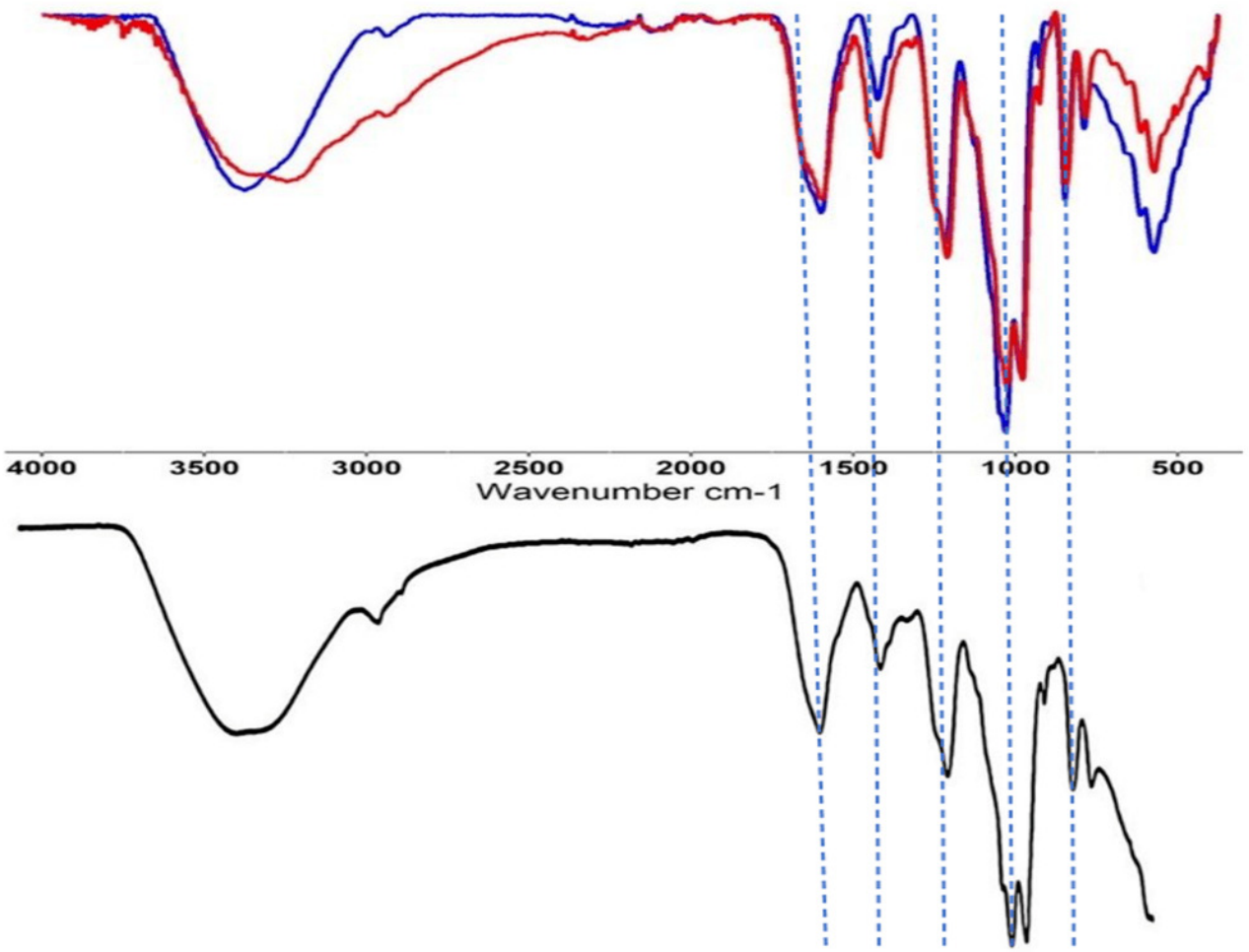

Figure 4

SEC-MALS chromatograms in Superose of AOx

(**A**) and HCl (**B**) extracts monitored by UV absorbance detector at 280 nm (green chromatogram), light scattering detector (LS, red chromatogram), Refractive Index detector (RI, blue chromatogram) detector and by MALS detector (average Molar Mass, black elution curve) (**A, B**).

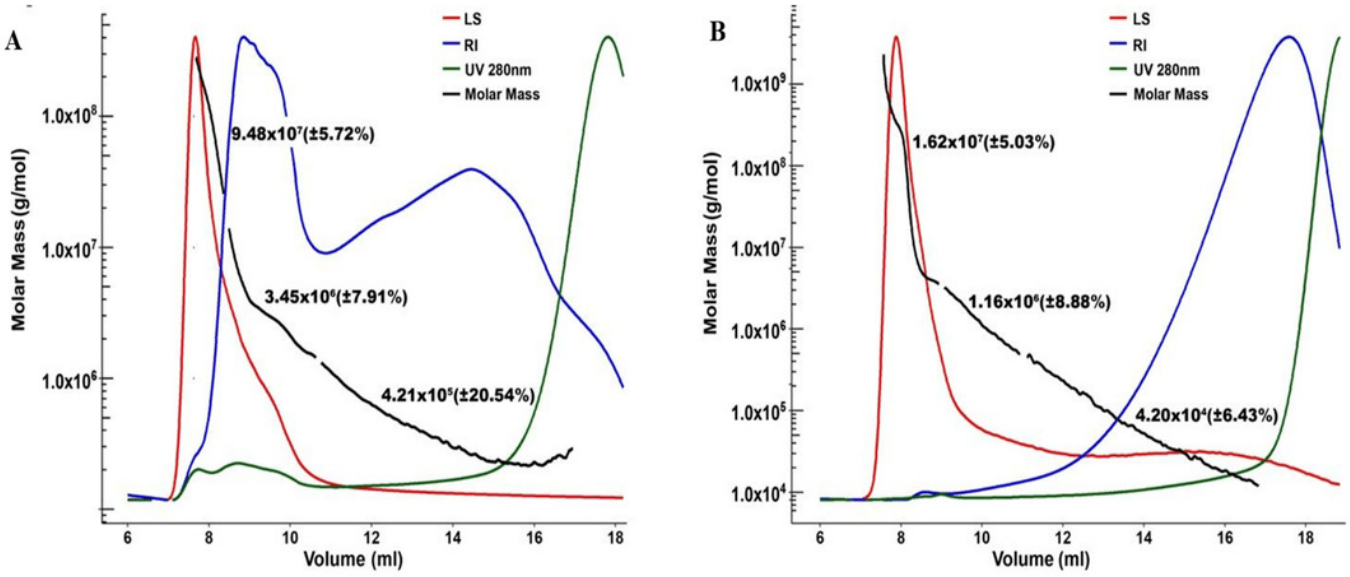

Figure 5

Structures of the main disaccharide units present in sulfated polysaccharides from *Ulva* sp. [39] .

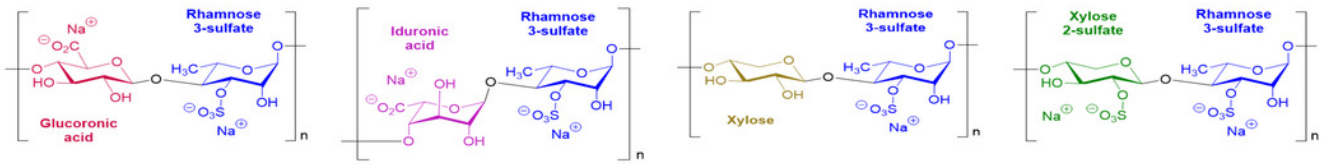

Figure 6

AEX-MALS chromatograms of ulvan extracts

AEX-MALS chromatograms of ulvan extracts from *Ulva sp*. using the AOx (**A, C**) and HCl (**B, D**) protocols, respectively. UV absorbance detector monitored at three wavelengths of 280 (blue chromatogram), 260 (red chromatogram), and 220 nm (pink chromatogram) (**A, B**). Chromatograms of the UV absorbance at 280 nm (green chromatogram), light scattering (LS, red) detector, and quasi-elastic light scattering (QELS, blue) detector are shown in **C & D** for the AOx, and HCl, protocols, respectively. P1 to P6 correspond to 6 different elution peaks.